Role of the Etna basement on surface faulting of the December 26, 2018, Mw 4.9 Fleri earthquake

Bella D.[1], Livio F.A.[2], Ferrario M. F.[2], Groppelli G.[3], Tringali G.[1], Boso D.[4], Blumetti A.M.[5], Di Manna P.[5], Vittori E.[5], Guerrieri L.[5], Porfido S.[6,7], Pettinato R.[1], Paradiso G.[1], Michetti A.M[2].

(1) Studio di Geologia Domenico Bella, Via N. Martoglio 13, 95024 Acireale (CT), Italy.

(2) Università degli Studi dell'Insubria, Dipartimento di Scienza ed Alta Tecnologia, Via Valleggio 11, 22100 Como (CO) Italy.

(3) C.N.R. - Istituto di Geologia Ambientale e Geoingegneria– sezione di Milano, Milano, Italy

(4) Geoexpert di Maria Rita Arcidiacono, Via M. Panebianco, 10, 95024 Acireale (CT), Italy.

(4) ISPRA – Geological Survey of Italy, Roma, Italy

(5) CNR-Istituto Scienze dell'Alimentazione Avellino

(6) INGV- Osservatorio Vesuviano Napoli.

Abstract

On December 26, 2018, an earthquake shook the eastern flank of the Etna Volcano (Sicily, southern Italy), with epicenter located near the Fleri village (focal depth less than 1 km, Mw 4.9) and was accompanied by widespread surface faulting. We surveyed and mapped the ground ruptures caused by the earthquake and collected structural data on the ground breaks orientation, displacement and on the fault fabric at surface. We here provide a detailed map of the surface faulting caused by the 2018 Fleri earthquake, and an accurate dataset of orientations and dimensioning data of the ruptured fault zones with associated slip vectors. We compare fault zone characteristics with near surface and deeper driving factors including the morphology of the topographic surface and of the buried top of basement, finding that the latter influenced the surface expression of faulting during the 2018 event. The topographic slope strongly influenced the fault strand pattern and slip orientation, above a critical slope angle of ca. 10°, in a sector close to the NE tip of the fault, the highest on the Mt Etna flank. The top surface of the basement is the local detachment floor for the sliding block and influences the amount of fault displacement at surface and the fault strands pattern. In particular, the presence of a lateral rise of the detachment surface to the south causes the sea-ward extrusion of the sliding block and the re-arrangement at surface of the fault strand pattern and deformations style, switching from shear faulting to a tensile failure. The surface rupture length (ca. 10 km) is consistent with previous empirical regressions calculated for volcano-tectonic events.

1 – Introduction

On December 26, 2018, at 3:19 a.m., an earthquake shook the eastern flank of the Etna Volcano (Sicily, southern Italy), with epicenter located near the Fleri village (focal depth less than 1 km, Mw 4.9; http://cnt.rm.ingv.it/en/event/21285011), accompanied by widespread surface faulting. This was the mainshock of an earthquake sequence (i.e., tens of Ml > 2.5 events) which started on December 23, 2018, with a concurrent phase of volcanic unrest that resulted in a series of explosive eruptions and a large dyke intrusion (Bonforte et al., 2019; De Novellis et al., 2019; Laiolo et al., 2019), which lasted till December 27 (Figure 1). The Fleri earthquake is the strongest instrumental shallow earthquake on Mt. Etna and provides unprecedented datasets for understanding active faulting in the European largest onshore volcano.

Since the morning after the mainshock, we surveyed and mapped the ground ruptures caused by the earthquake along the Fiandaca Fault and nearby capable segments, and collected structural data on the ground breaks orientation, displacement and on the fault fabric at surface. For the first time, the scientific community had the opportunity to document a volcano-tectonic surface faulting event in the Etnean area with modern field techniques coupled with remotely-sensed data (InSAR-detected ground displacement).

Earthquake surface faulting at Mt. Etna volcano has been well documented since 1800's through macroseismic investigations and studied in depth in the past decades (e.g., Riuscetti and Distefano, 1971; Azzaro et al., 1998; Azzaro, 1999). Paleoseismological studies constrained Holocene slip-rates along the Moscarello and Pernicana Faults (Azzaro et al., 2000; Ferreli et al., 2002). Recent seismic events, as the October 25, 1984, Fleri earthquake (Mw 4.4; Benina et al., 1984; Patanè and Imposa, 1995), and the October 29, 2002 Santa Venerina event (Mw 4.4; Monaco et al., 2005; Blumetti et al., 2007), have been investigated in detail also with increasing instrumental seismology and geodetic accuracy, but still lack of systematic field mapping and structural measurements associated with remote sensing data.

Fault zone fabric at surface in volcano-tectonic environments is peculiar, since strongly dependent on the local geological, geomorphological and rheological setting. In particular, capable faults at Mt. Etna (Azzaro et al., 1998) are characterized by i) very shallow earthquake foci (< 1 km), ii) the concurrent role of gravity in driving shallow crustal deformation (e.g., Borgia et al., 1992, Carveni and Bella, 1994; Carveni et alii, 2005, Bella et alii 1996, Carveni et alii, 1997; Groppelli and Tibaldi, 1999; Lundgren et al., 2004; Neri et al., 2007; Bonforte et al., 2011; Chiocci et al., 2011; Groppelli and Norini, 2011; Azzaro et al., 2011), iii) the co-existence of locked and creeping segments during the inter-seismic phase, iv) significant post-seismic slip released after coseismic events, and v) the complexity of the near surface geological setting (i.e.-volcano dynamics and morphology, thickness of the volcanic deposits and morphology and rheology of the underlying sedimentary basement, e.g., Branca et al. 2011; Branca and Ferrara, 2013).

In this paper, we provide a detailed map of the surface faulting caused by the 2018 Fleri earthquake, and an accurate dataset of orientations and dimensioning data of the ruptured fault zones with associated slip vectors. Our survey dataset is complementary to another recently published mapping of the ground breaks (Civico et al. 2019) that was surveyed independently still with consistent results. Data are examined in order to constrain some of the several concurrent variables that control the fault zone fabric. We analyze, through a GIS approach, the role of geologic, geometric, and morphological factors (i.e., primary vs distributed partitioning of faulting, near-surface lithology, trends along strike and relationship with terrain slope and aspect) in determining the surface expression of faulting and discuss this analysis in the framework of the fault displacement hazard assessment.

2 - Geological and seismotectonic setting

2.1 Geological setting

The Fleri earthquake occurred on the eastern flank of Mount Etna volcano, located in the hanging wall of the Apennine–Maghrebian accretionary prism, close to the Hyblean–Malta Escarpment (e.g., Doglioni et al., 2001; Barreca et al., 2019). Mt Etna is around 3300 m high and is characterized by frequent explosive and effusive basaltic activity, mainly lava flows from the summit craters and the surrounding monogenetic craters and scoria cones. Recently Branca and Ferrara (2013) published the palaeo-topography of the Etna basement, showing a volcanic pile reaching 2500 m below the summit crater area and characterized by a depressed area, to the east, filled by clay and siltstone of the Pleistocene Argille grigio-azzurre Formation (Lentini et al., 2006).

The volcanic activity started around 500 ka (De Beni et al. 2011) with submarine eruption in the Aci Castello area, whereas the present morphology has been built more recently since the Ellittico volcano (56 ka, De Beni et al. 2011).

From the geodynamic point of view, there are different models, some of them outline the role of the Timpe fault system, the inland prosecution of the Malta Escarpment, a Mesozoic structure reactivated during Late Pleistocene (Lanzafame and Bousquet 1997; Nicolich et al. 2000; Doglioni et al. 2001; Argnani and Bonazzi 2005; Argnani et al., 2013) as the main lithospheric structure driving the magma to the surface. At the opposite, other models consider the Timpe fault system as the results of gravitational instability affecting the margin offshore Mt. Etna (Chiocci et al. 2011; Gross et al., 2016; Urlaub et al. 2018). Recently Firetto Carlino et al. (2019) propose a main structure E-W striking affecting the southern margin of Mt. Etna and the Timpe fault system as the deformation above deeper splays related to the regional-scale tectonics.

The eastern and southern flanks of the Etna volcano are continuous sliding towards east and south (e.g. Borgia et al., 1992; Tibaldi and Groppelli, 2002; Solaro et al., 2010: Bonforte et al., 2011; Groppelli and Norini, 2011; Norini and Acocella, 2011; Ruch et al. 2012; Azzaro et al., 2013). For this reason, the SE flank is characterized by frequent, low magnitude and very shallow seismic events (Figure 1). Commonly, hypocentral depths are shallower than 1–2 km, hence within the volcanic blanket, which rests on relatively shallow bedrock (Pleistocene foredeep clays belonging to the Argille grigio-azzurre Formation; Branca et al., 2011; Branca & Ferrara, 2013). Therefore, notwithstanding its small magnitude, the seismic activity locally induces remarkable shaking and ground surface ruptures. At the same time, frequent fault creep phenomena take place along well-defined structures, sometimes, but not always, associated with seismic events and/or volcanic eruptions (Azzaro et al., 1998).

2.2 Recent deformation along the Timpe fault system

The maximum coseismic deformation occurs along the faults belonging to the Timpe fault system. The Moscarello fault (MOS in Figure 1) has a length of 12 km with a scarp up to 125 m high. This is the minimum displacement of 126.4 ± 4.8 ka old volcanic deposits (Moscarello formation, Timpe phase —De Beni et al., 2011), suggesting a long-term slip rate higher than 1 mm/yr. Paleoseismological analysis carried out across the fault revealed a Holocene vertical slip rate of 1.4–2.7 mm/yr (Azzaro et al., 2000; Ferreli et al., 2000; 2002). During the past two centuries, this fault has generated four seismic events (in 1855, 1865, 1911 and 1971) with intensities of VII–VIII to X MSK (Medvedev–Sponheuer–Karnik). All these events were accompanied by surface ruptures up to 6 km long and measured dip-slip displacements between 25 and 90 cm. The San Leonardello fault (LEO in Figure 1), also belonging to the Timpe fault system, has a length of about 9 km and shows fault scarps up to 25–30 m high in alluvial and volcaniclastic deposits much younger than 10 ka BP (Calvari and Groppelli, 1996;

Monaco et al., 2010; De Beni et al., 2011). This fault is considered the source of the 1881, 1920, 1950, 1989 earthquakes with intensities VII–VIII MSK. The 1920 and 1950 events were characterized by vertical displacement between 30 and 60 cm and minor strike-slip dextral components of a few centimeters (Lo Giudice and Rasà, 1992; Monaco et al., 1997; Azzaro, 1999, 2004). The Linera fault (LIN, in Figure 1) is partially hidden by the historical (i.e. 1329 A.D.) lava flows and extends from the village Santa Tecla almost up to the town of Zafferana, farther than revealed by the field evidence given by the cliff named "Timpa di Santa Tecla". This is demonstrated by repeated historical surface faulting occurred during the 1865, 1879, 1914, 1952, 1973 and 1981 events. In particular, the 1914 Linera earthquake caused the most relevant faulting in the Etna area, with rupture length of 6,5 km and 25-40 cm of throw (Ghersi et al., 1914; Platania, 1915; Sabatini, 1915). The Santa Venerina fault (VEN, in Figure 1) is also mostly hidden, having geomorphic expression only in its southern part, (south of San Giovanni Bosco village), but causing extensive surface rupture in 1879 and 2002, for a length of 6 and 5 km respectively. The Acireale – Santa Maria la Scala fault (SCA, in Figure 1) belongs to the southern part of the Timpe system. It has a length of about 7 km and shows rectilinear fault scarps up to 120 m high in about 130 ka old volcanic deposits (Timpe phase: De Beni et al., 2011). This NNW trending fault is characterized by oblique kinematics with right-lateral component (Monaco et al., 1997).

The NW-SE trending Fiandaca fault (FIA) belongs to the Timpe system, stretching from Fleri to the Aci Catena area with a curvilinear trace, a dominant right-lateral, strike-slip kinematics, and an overall length of ca. 8 km. In the southern part, it connects to Aci Catena (CAT) and Aci-Platani (PLA) faults through several fault splays and multiple parallel scarps. Typically, the FIA trace is marked by minute but clear evidence of long-term displacement, due to local vertical component of slip. Before the 2018 earthquake, the FIA activity has been demonstrated by several, well-documented historical and instrumental surface faulting earthquakes, in particular in 1875, 1894, 1907, 1914, 1984, 1997 (Figure 1).

At the southern termination of the FIA fault, a distinct N-trending, E-dipping morphological flexure marks the transition to the PLA fault. Known since 1879 (Baratta, 1901), the PLA is ca. 6 km long, and in its southern part, approaching the coastline, its strike changes to NNE-SSW. Its kinematics is normal, east side down, with slip by events of aseismic creep or local earthquakes (Silvestri, 1879a,b; Patanè Musumeci, 1886).
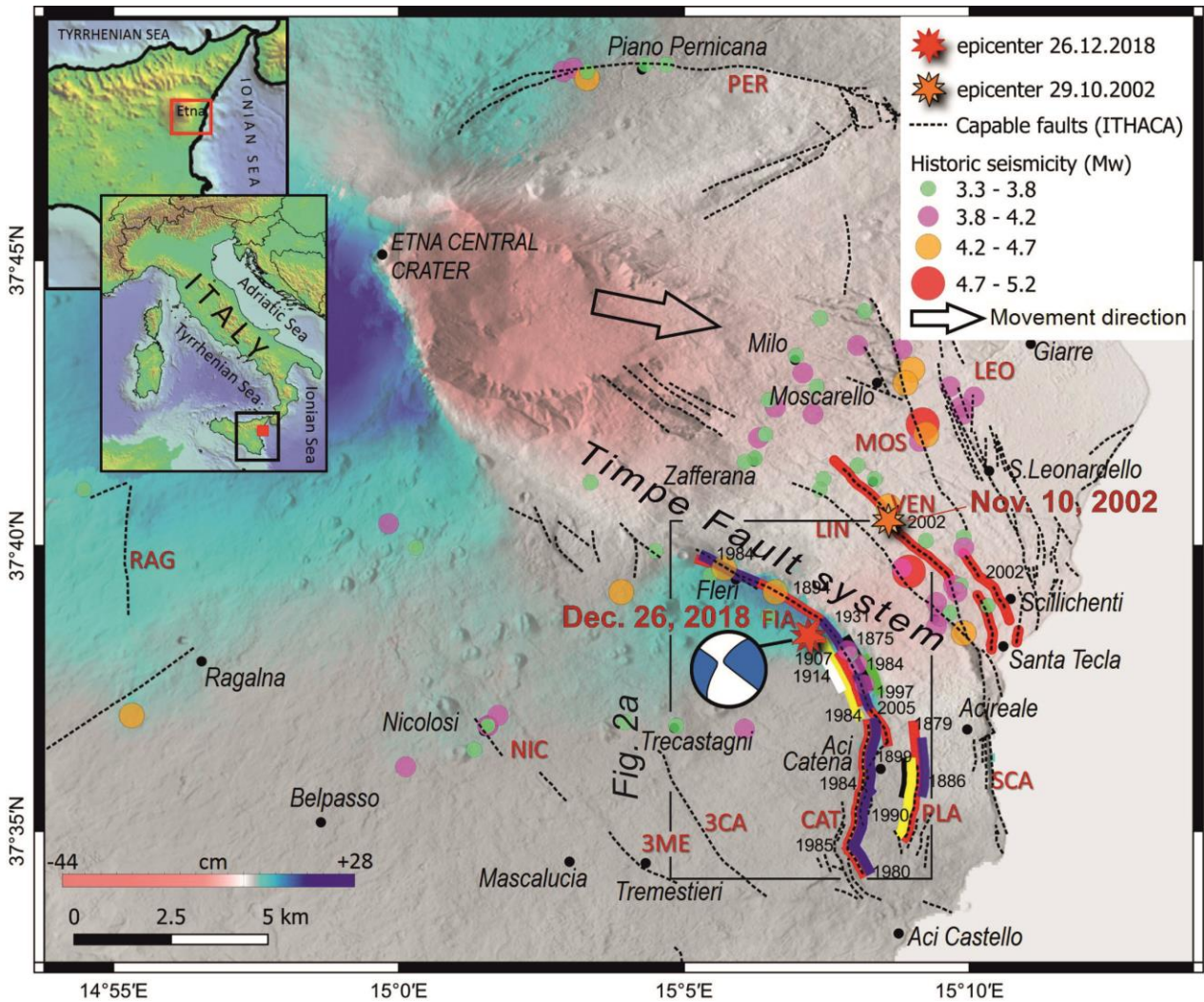
142

143 **FIGURE 1: REGIONAL CAPABLE FAULT MAP OF M. ETNA; COLOR BANDS INDICATE THE HISTORICAL SURFACE RUPTURES ALONG THE**
144 **FIANDACA AND ACI CATENA FAULTS; THE EPICENTERS OF THE NOV. 10, 2002 (S. VENERINA) AND OF THE DEC. 26, 2018 (FLERI)**
145 **EARTHQUAKES ARE REPORTED TOGETHER WITH HISTORICAL SEISMICITY (CPTI CATALOGUE, ROVIDA ET AL. 2016). MAJOR FAULTS**
146 **ARE LABELLED AS FOLLOWS: FIA, FIANDACA; PER, PERNICANA; CAT, ACI CATENA; PLA, ACI PLATANI; RAG, RAGALNA; LEO, SAN**
147 **LEONARDELLO; MOS; MOSCARELLO; LIN, LINERA; VEN, SANTA VENERINA; SCA, SANTA MARIA LA SCALA - ACI REALE; 3ME,**
148 **TREMESTIERI; 3CA, TRECASTAGNI; NIC, NICOLOSI.**

3 – Methods and datasets

149

150

3.1 – Field survey

151

152 Field surveys started within hours of the December 26, 2018 earthquake. We took advantage of information
153 already available before the event, timely generated after it, including: i) a digital elevation model at 10 m
154 resolution (Tarquini et al., 2012); ii) the database of the active and capable faults (ITaly HAzard from CApable
155 faults - ITHACA, see Data and Resources); iii) interferograms generated from Sentinel 1 SAR imagery (images
156 taken on December 22 and 28, processed with the SNAP software from ESA) and (iv) information collected
157 through interviews with local inhabitants. A detailed and complete interferometric analysis, which was outside
158 the aims of the present study, is found in De Novellis et al. (2019).

159 We systematically surveyed the epicentral region looking for any kind of coseismic effects: our collected data
160 refer to newly-formed ground breaks affecting roads and sediments; small mass movements mainly occurring

along road shoulders or stone walls were recorded as well. Our efforts focused on the FIA and PLA faults, where most of the damage was located.

Rupture traces were mapped on topographic maps at 1:5,000 scale or using iPad mini equipped with iGis software and Google Earth images. For each observation point, we collected an extensive photographic documentation and took the following measurements, whenever possible, on ground breaks: i) strike and length of the ground break; ii) heave (horizontal offset); iii) throw (vertical offset); iv) net displacement; v) slip vector orientation from piercing points (i.e., trend and plunge); v) fault plane orientation and slip on fault, if available. When information was available and reliable, we measured the ground ruptures strike, length, slip vector and net slip amount. Alternatively, when only partial constraints were available, we reported at least the maximum heave or throw. All orientation measurements are expressed in Clar's notation and the complete dataset is available in the electronic supplement of this article (NOT PROVIDED HERE).

The coordinates of observation points were collected by means of a handheld GPS with an accuracy of ca. 2 meters. Displacements and lengths were measured with a geological compass and a ruler or measuring tape; the obtained accuracy can be estimated in ca. 1 cm. Net displacements and slip vectors were measured only if clear piercing points were available on the two sides of the rupture.

The investigation of the epicentral region during an ongoing seismic crisis presents some challenges. Beside operative problems (e.g., road closures, access to private properties), the surveys should be done as soon as possible after the earthquake, because minute coseismic evidence can be easily erased by degradation and/or road repairs. Post-seismic slip, creep processes and/or the possible occurrence of further seismic events can alter the amount of displacement, which implies that an acquired measure may represent a cumulative effect. All the field surveys were realized within one month since the earthquake, involving 14 people, for a field survey that lasted ca. 30 days after the earthquake. Most relevant to the issues highlighted above, part of our team is living in the epicentral area; this allowed us to solve relevant logistic issues (property access, interview with local witness) and provided timely and extremely accurate update on the afterslip evolution during the weeks following the mainshock.

3.2 – Database analysis

All the data have been organized in a GIS database (WGS84 - UTM Zone 33N, available in the electronic supplement to this article – NOT PROVIDED HERE). We shared a common survey methodology for mapping and recording data; anyway, once collected, all data were further processed and verified, to avoid duplication and inexact formats and to obtain a properly organized database. This database is made up of 273 observation points, mainly located along the FIA fault.

We divided the observed ruptures along the FIA and PLA faults into 3 segments (namely the A, B and C segments in Figure 2), according to previous information (e.g., ITHACA fault strands) and a change in the fault strike. For each segment, we projected the data location on a baseline, according to the average strike of the observed ruptures (Figure 2), and derived along-strike profiles for selected variables (e.g., slip azimuth, strike, displacement); fault width was measured perpendicularly to the baseline every 50 m.

We derived slope and aspect rasters from a DTM (10 m of grid spacing – Tarquini et al., 2012) and from a DEM of the top of basement (100 m of grid spacing derived from the elaboration of 50 m equidistance contour lines published in Branca and Ferrara, 2013). These layers were compared with fault slip data and faulting characteristics by sampling the average value of each layer on a 100 x 100 m moving window centered on each observation point.

4- Results: ground breaks distribution and fault fabric analysis

Figure 2 shows the ground breaks mapped after the 2018 earthquake and the position of segments A, B and C; the length of the mapped ruptures is about 10 km. Measured displacements are generally of a few cm, locally reaching up to 30 cm (Figure 3). A synthetic rendering of the data distribution is given in Figure 4, where we report the values of strike and slip orientations, color-coded according to the three segments. A brief description is provided below.

A segment:

It runs from the SW sector of M. Illice through the hamlet of Fleri, up to Pennisi. The average strike is N297, length about 3500 m. We identified 86 ground breaks, which could be generally followed for tens of meters (average length: 102 m, maximum length of individual ground breaks: 1010 m). Fractures are arranged as anastomized in the NW sector, passing to a left-stepping en-echelon pattern near the Fiandaca segment; the rupture zone width is 230 m on average, but reaches up to 1.5 km. The distribution of ground breaks strikes is quite wide, centered on values close to N330-340 and with a secondary mode striking ca. NE-SW (Figure 4b and d). The angle between each ground break strike and its slip vector dip direction (i.e., the fault obliquity, Figure 4c) ranges between 42º and 82º, indicating the coexistence of normal to transtensive dextral faults, with an irregular spatial distribution of the data.

B segment:

It runs from Pennisi through Santa Maria la Stella with an average strike of N332 and a length of 4100 m. We mapped 54 ground breaks, which are on average shorter than those in the Fleri segment (average length: 84 m) and distributed in a much narrower zone (average fault width: 28 m). This segment is fully arranged in a left-stepping pattern with shorter average length of each ground rupture. The SE tip of this segment shows a horsetail splaying at its southern tip, consistent with the dextral component of movement. Ground breaks regularly strike N340 with a secondary mode trending N20, representing Riedel faults associated to the main fault zone. Fault obliquity ranges between ca. 60º and 80º, with an average value of ca. 70º, indicating a transtensive accommodation of strain along localized shear zones.

**C segment:**

It runs from S. Maria la Stella to the southernmost tip of the rupture, with an average strike of N160 and a length of 2800 m. The fault width is highly variable, with values decreasing from north to south. Ground ruptures are typically organized in a single linear trace, with a rather narrow fault width. Ground breaks strike N350-360 with a secondary mode trending N30. Kinematics are normal, east side down, or purely dilational fractures, as illustrated by the numerous depressions in the paving of the houses. In the southern part, at the limit with agricultural land, traces of fracturing were found along the boundary walls.
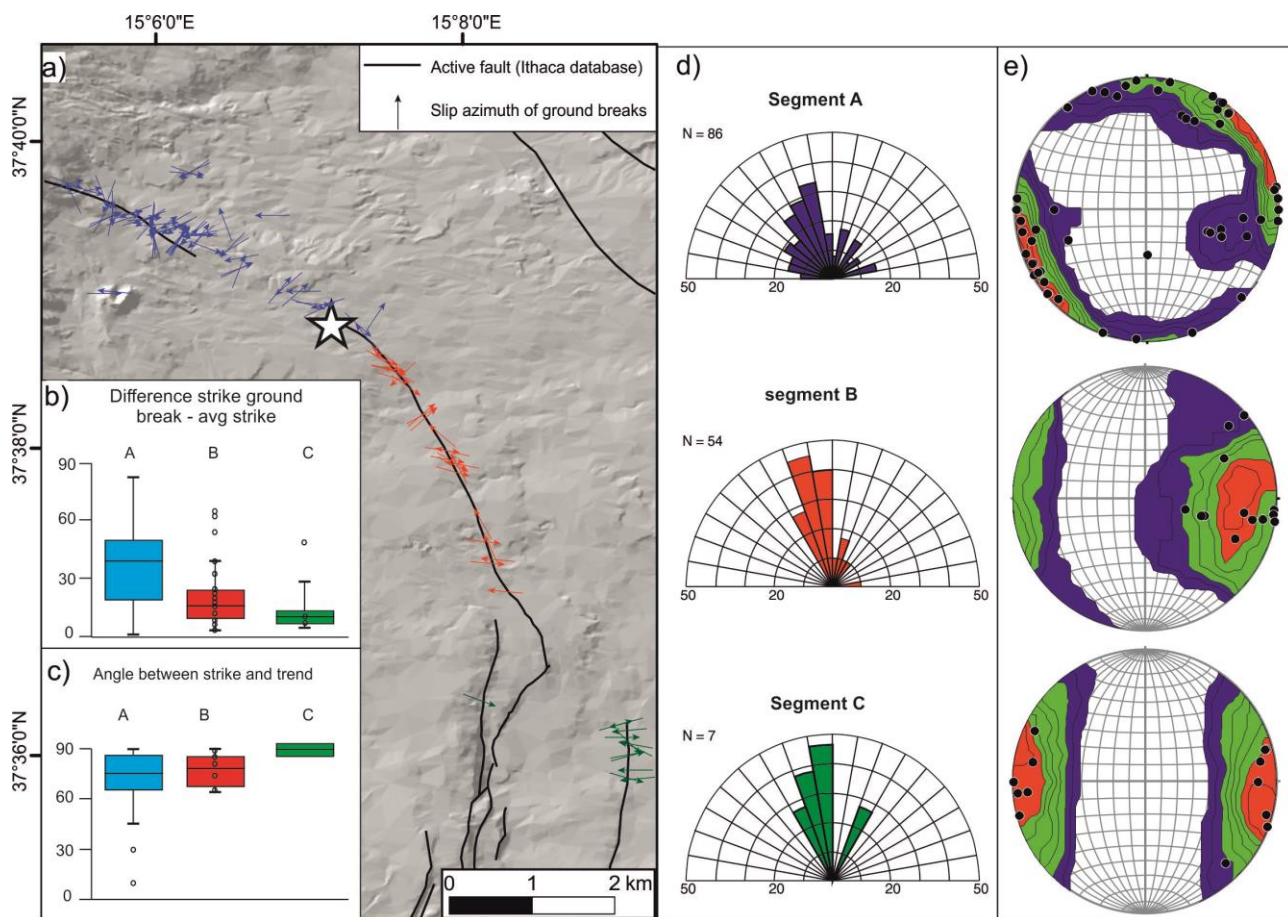
238
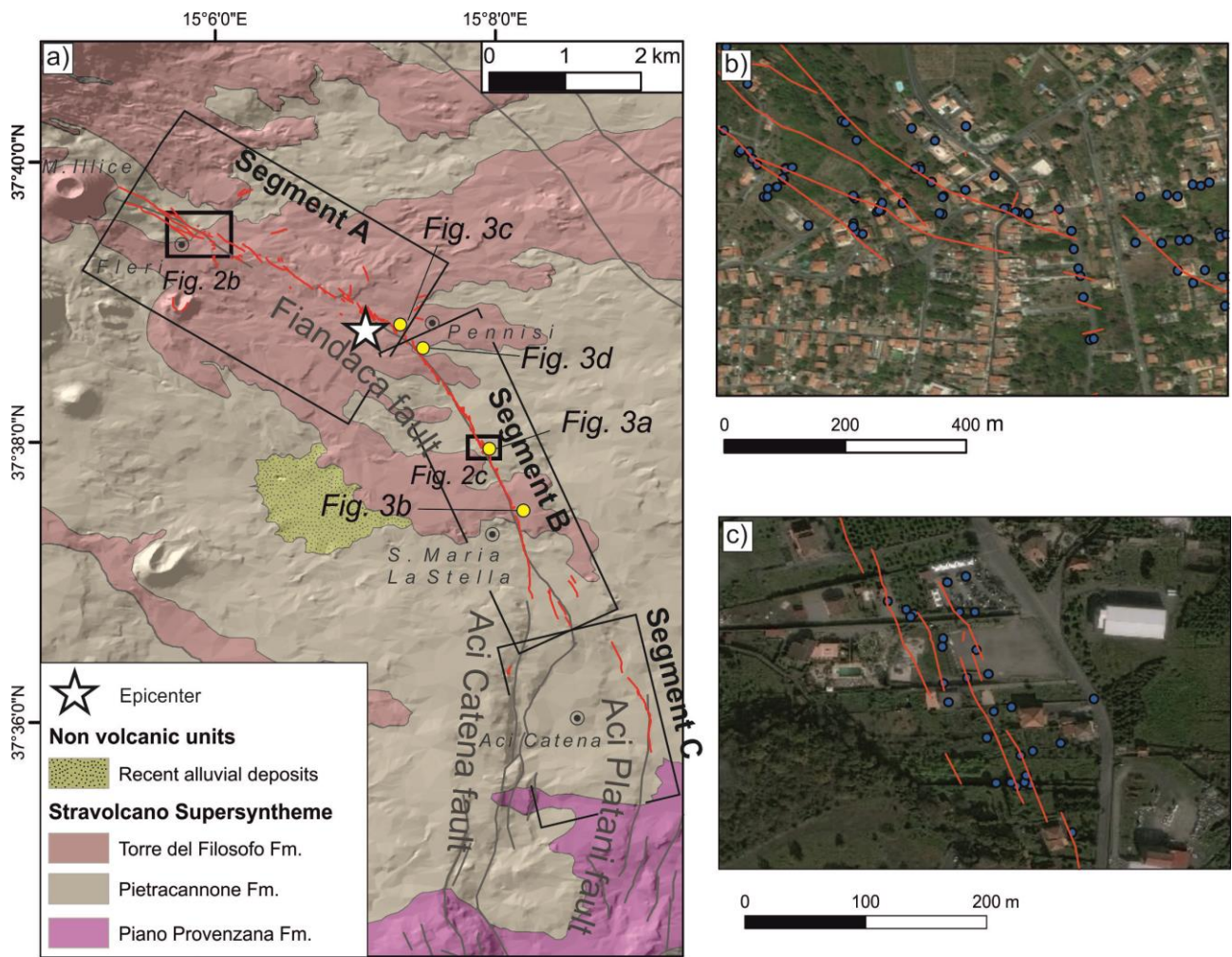
FIGURE 2: A) GEOLOGICAL BASEMAP (AFTER BRANCA ET AL., 2011; MODIFIED) AND GROUND BREAKS MAPPED AFTER THE 2018
EARTHQUAKE; B) ZOOM ON THE FLERI AREA; C) ZOOM ON THE PENNISI – SANTA MARIA LA STELLA AREA.
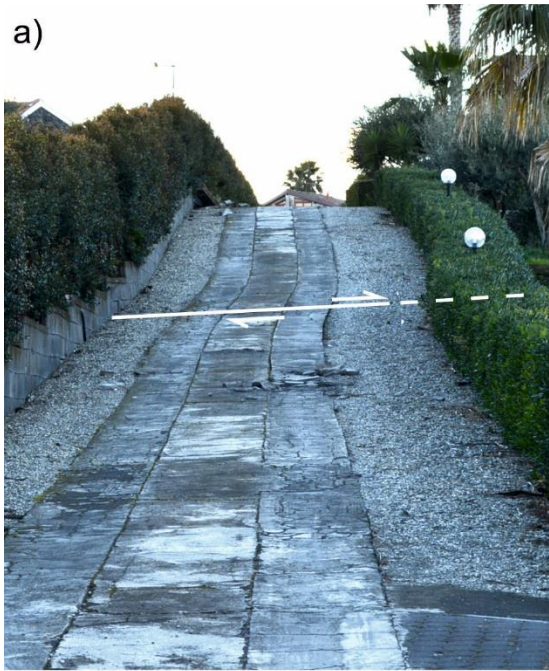
FIGURE 3: FIELD PHOTOS OF GROUND CRACKS IN ASPHALT AND PAVED ROADS (A, B) AND SOILS (C, D). LOCATION IS SHOWN IN FIGURE 2.

FIGURE 4: A) MAP OF THE SLIP AZIMUTH OF GROUND BREAKS. B) BOXPLOT SHOWING THE DIFFERENCE BETWEEN THE STRIKE OF MAPPED GROUND BREAKS AND THE AVERAGE STRIKE OF EACH SEGMENT. C) BOXPLOT SHOWING THE ANGLE BETWEEN THE STRIKE OF GROUND BREAKS AND THE TREND OF SLIP VECTORS. D) STRIKE OF MAPPED GROUND BREAKS. E) SLIP VECTORS MAPPED ALONG THE THREE SEGMENTS.

5. Discussion: factors affecting surface faulting style

In order to explore possible factors affecting the style of surface faulting, we compared fault zone characteristics with near surface and deeper driving factors including the morphology of the topographic surface and of the buried top of basement, finding that the latter strongly influenced the surface expression of faulting during the 2018 event. Instead there is no correlation with surface geology (fig. 2), mainly because of the recent age and the similar rheology of the lava flows affected by ground ruptures.

Firstly, we compared the fault zone width with the topographic slope (Figure 5), observing that the largest fault zone is located in segment A, closest to the flank of M. Etna, where an irregular topography and relatively high slope angles are present. Segment B, conversely, with a topographic slope angle smaller than 10°, shows a narrower fault zone, with a limited number of fault strands across strike. Along the southernmost sector of Segment B, between 6 and 8 km along-distance (Figure 5a), fault width significantly increases without a corresponding change in the topographic slope. These points lie where the left-stepping en-echelon pattern of the segment B passes to a horsetail splaying and kinematics deviates from transtensional to purely normal.
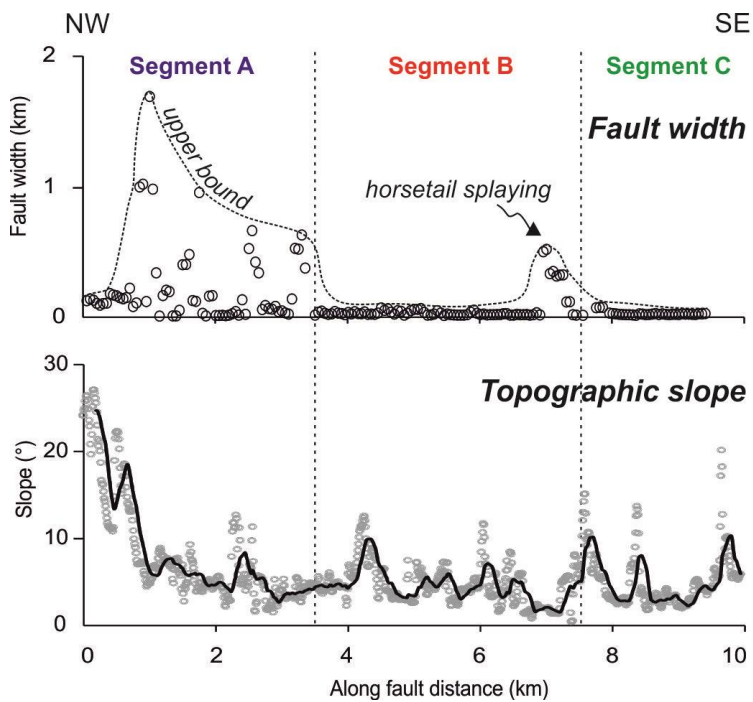
267 We compared the faulting characteristics with the geometry of the top of basement (i.e., the top of Pleistocene
268 clays and siltstones underlying the volcanic complex, as mapped after Branca and Ferrara, 2013): an underlying
269 weak horizon on which shallow deformation is rooted and considered as a detachment surface for the sliding
270 block of the Mt Etna eastern flank. The area lies on a basement that gently dips to the SE in the northern sector
271 and, due to deformation induced by contractional tectonics, it is deformed in an elongated depression centered
272 at ca. N37º38' bordered, to the south, by a steep E-W trending scarp (Figure 6a). We calculated the thickness of
273 the volcanic pile as the difference between a DTM and the top of basement surface.

274 We found that displacement of ground ruptures is correlated with the thickness of the volcanic units, with a
275 maximum slip along the segment B, where the depression depocenter is located (Figure 6b). Minimum slip is
276 associated with segment C and intermediate values are recorded along the segment A. Such a correlation is
277 expected if we consider a simple kinematic model of listric faults accommodated by hanging wall collapse in a
278 rollover anticline (Figure 6c). The models were calculated in the 2D MOVE structural software. Near surface
279 displacement would be proportional to the thickness of the section cut by the fault ramp.

280 The geometry of the top of basement is also the primary factor affecting the orientation of fault slip and strike.
281 The NE block of the fault moved parallel to the average top of basement aspect (to the SE) and, locally, the strike
282 of the fault strands is parallel too. The southernmost sector of the segment B, where the fault zone width
283 increases and fault strands gradually rotate from NW-SE to N-S, lies where the top of basement steeply dips to
284 the north, almost opposite to the average slip dip direction. The two sectors of the segment B are clearly
285 clustered also if we consider the strike of fault strands plotted against the aspect of the underlying basement
286 (Figure 6d). The strike of fault strands lying on a N-dipping basement ranges between N and NNW whereas NE to
287 SE trending ground ruptures, dominating in the other sectors, are absent. We suppose that the strong influence
288 of the geometry of the top of the basement on the ground ruptures orientation can be partly ascribed to the fact
289 that this horizon is a particularly weak layer, as suggested also by numerical modeling (Apuani et al. 2013),
290 implying a local stress re-orientation (e.g., Faulkner et al. 2007).

11

The rise of the top of basement in the southern sector causes the sliding block to be extruded eastward, with the development at surface of normal faults and pure dilational fractures in the segment C.
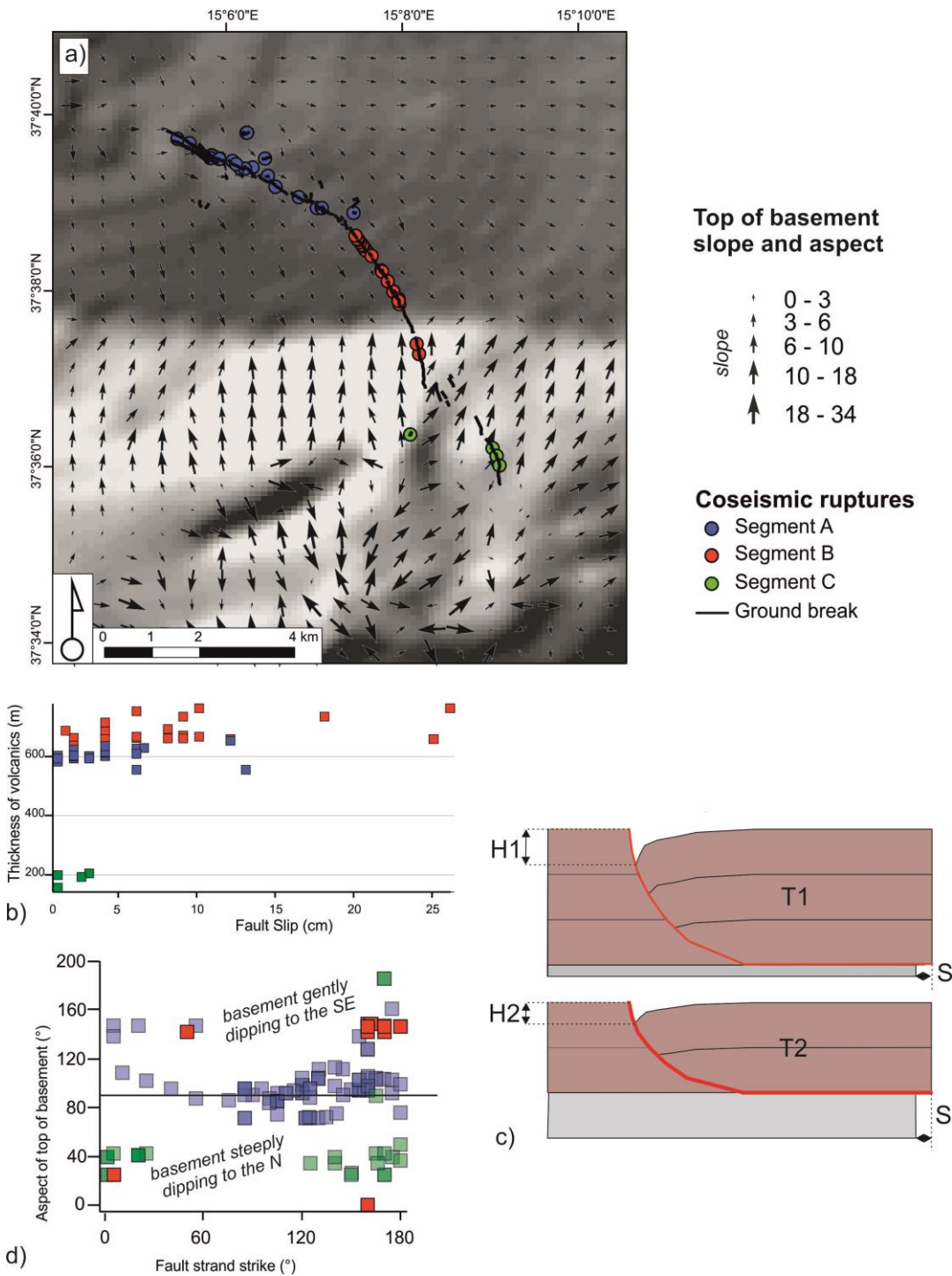
FIGURE 6: A) GROUND BREAKS AND MEASUREMENTS POINTS (COLOR CODED ACCORDING TO SEGMENTS) PROJECTED ONTO THE SHADED RELIEF MODEL OF THE TOP OF BASEMENT; ARROWS INDICATE ASPECT AND SLOPE OF THE SURFACE; B) FAULT SLIP VERSUS THICKNESS OF THE VOLCANIC COMPLEX OVERLYING THE BASEMENT; C) SKETCH MODEL OF TWO NORMAL LISTRIC FAULTS OF SLIP (S) DETACHED AT TWO DIFFERENT DEPTHS (T1 AND T2); THE ACCOMMODATION OF DISPLACEMENT AT SURFACE, ACCORDING TO A SIMPLE SHEAR KINEMATIC MODEL RESULTS IN A FAULT THROW (H1 AND H2) PROPORTIONAL TO THE DETACHMENT DEPTH; THE TWO MODELS WERE CALCULATED IN THE 2D MOVE STRUCTURAL SOFTWARE (COURTESY OF PETROLEUM EXPERTS) AND REDRAWN; D) FAULT STRAND STRIKE VERSUS THE ASPECT DIRECTION OF THE TOP OF BASEMENT.

6 – Conclusions

We here document a detailed mapping of the ground ruptures associated with the December 26, 2018, Fleri earthquake and provide a dataset of structural data on fault slip and on the orientation of fault strands.

Our observations on the extent and sense of movement at surface are consistent with the model of a block sliding to the ESE and detached at shallow levels above a weak layer of mudstones and siltstones underlying the volcanic complex (e.g., Carveni and Bella, 1994; Carveni et al. 1997, 2005). Seismological data consistently indicate a less than 1 km hypocentral depth. It is noteworthy that the inversion of InSAR-detected ground deformation results in a shallow source with an estimated fault slip of 60-70 cm located mainly at a depth of ca. 700 m (Bonforte et al., 2019; in a range of 400 – 1000 m according to De Novellis et al., 2019), i.e., corresponding to the thickness of the volcanic pile at the epicentral location.

By means of a GIS approach, we spatially compare structural data with other variables and conclude that the topographic slope strongly influenced the fault strand pattern and slip orientation above a critical slope angle of ca. 10°. The sector mostly affected by this variable is close to the NE tip of the fault, i.e., the segment A, the highest on the Mt Etna flank. We also find that the top surface of the basement is the local detachment floor for the sliding block and influences the amount of fault displacement at surface and the fault strands pattern. In particular, the presence of a lateral rise of the detachment surface to the south causes the sea-ward extrusion of the sliding block and the re-arrangement at surface of the fault strand pattern and deformations style, switching from shear faulting to a tensile failure. This transition in the failure mode can be mainly ascribed to the change in overburden load as the thickness of the volcanic cover decreases. This is well predicted by physical models (Kettermann and Urai, 2015) and observed in other volcano-tectonic settings (Kettermann et al., 2019).

The mapped fault strands extend for a length of ca. 10 km. The surface rupture length is consistent with previous empirical regressions calculated for volcano-tectonic events (Riuscetti and Distefano, 1971; Azzaro, 1999; Mohammadioun and Serva, 2001; Azzaro et al. 2017; Figure 7) and with recent observations on other volcano-tectonic shallow events in Italy: i.e., the October 29, 2002, S. Venerina earthquake, Mw 4.4; and the August 21, 2017, Ischia earthquake, Mw 3.9 (Nappi et al., 2018; Figure 7). Arguably, the long-documented history of coseismic and aseismic surface faulting at Mt. Etna follows an entirely different scaling law if compared with most shallow crustal earthquakes elsewhere in the world. The Fleri earthquake provides therefore new perspectives on the physical and rheological processes controlling this law.
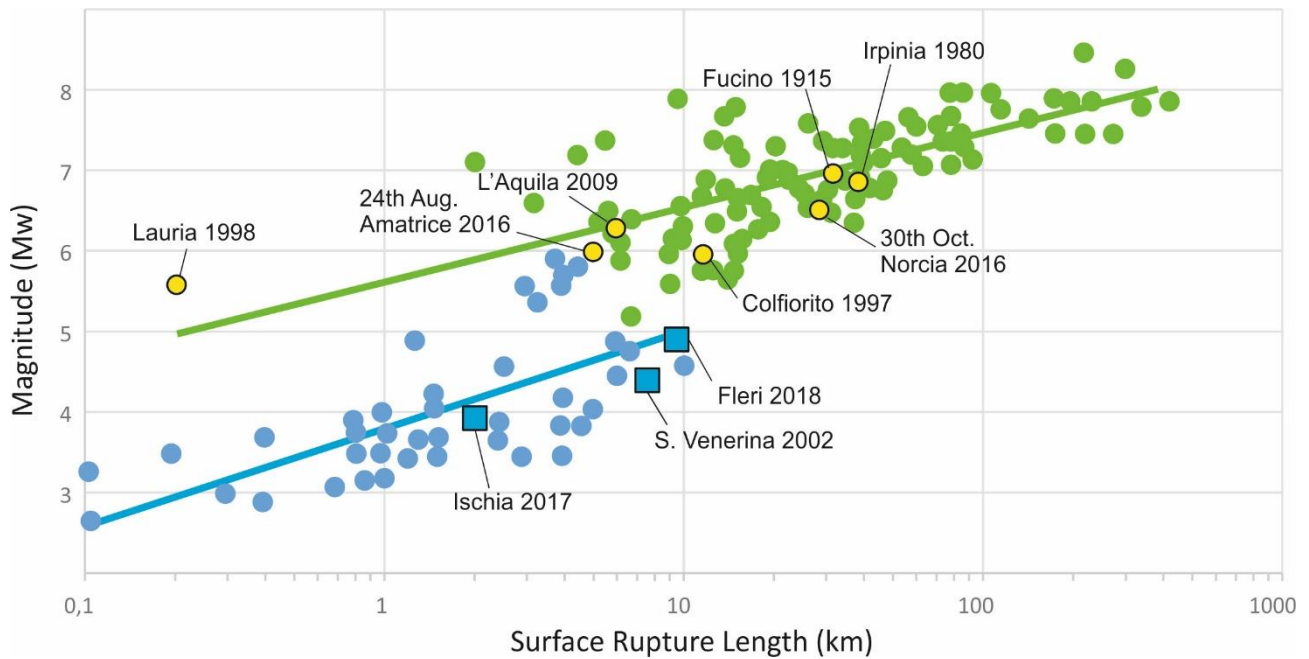
330

331 **FIGURE 7: MAGNITUDE PLOTTED VERSUS SURFACE RUPTURE LENGTH: SHALLOW SEISMIC EVENTS FROM THE ETNA VOLCANO (BLUE**
332 **DOTS, AFTER AZZARO, 1999) COMPARED WITH THE DATA (GREEN DOTS) FROM WELLS AND COPPERSMITH (1994) AND SELECTED**
333 **ITALIAN EARTHQUAKES (YELLOW DOTS). IN THIS GRAPH WE INCLUDED ALSO THE AUGUST 21, 2017, ISCHIA EARTHQUAKE - MW 3.9**
334 **(BLUE SQUARE; NAPPI ET AL., 2018) AND THE OCTOBER 29, 2002, S. VENERINA EARTHQUAKE (MW 4.4; BLUMETTI ET AL., 2007).**

Data and resources

336 Seismological data were retrieved from the INGV website at http://cnt.rm.ingv.it/event/21285011 (last
337 accessed November 8, 2019). The Ithaca database of capable fault is publicly available at
338 http://sgi2.isprambiente.it/ithacaweb/viewer/ last accessed, November 8, 2019).

339 The electronic supplement to this article (NOT PROVIDED HERE) includes shapefiles of the ground breaks and
340 point observations.

Acknowledgments.

References

Argnani, A., & Bonazzi, C. (2005). Malta Escarpment fault zone offshore eastern Sicily: Pliocene‐Quaternary tectonic evolution based on new multichannel seismic data. Tectonics, 24(4).

Argnani, A., Mazzarini, F., Bonazzi, C., Bisson, M., & Isola, I. (2013). The deformation offshore of Mount Etna as imaged by multichannel seismic reflection profiles. Journal of Volcanology and Geothermal Research, 251, 50-64.

Azzaro, R., 1999. Earthquake surface faulting at Mount Etna volcano (Sicily) and implications for active tectonics. Journal of Geodynamics, 28, 193–213.

Azzaro R., (2004) – Seismicity and active tectonics in the Etna region: contraints for a seismotectonic model – in Bonaccorso A., Calvari S., Coltelli M., Del Negro C., Falsaperla S. (edts) Mt Etna: volcano laboratory, American Geophysical Union Monograph 143, 205-220.

Azzaro, R., Ferreli, L., Michetti, A. M., Serva, L., & Vittori, E. (1998). Environmental Hazard of Capable Faults: The Case of the Pernicana Fault (Mt. Etna, Sicily. Natural Hazards, 17(2), 147-162.

Azzaro, R., Bella, D., Ferreli, L., Michetti, A. M., Santagati, F., Serva, L., & Vittori, E. (2000). First study of fault trench stratigraphy at Mt. Etna volcano, Southern Italy: understanding Holocene surface faulting along the Moscarello fault. Journal of Geodynamics, 29(3-5), 187-210.

Azzaro, R., A. Bonforte, S. Branca, and F. Guglielmino (2013), Geometry and kinematics of the fault systems controlling the unstable flank of Etna volcano (Sicily), J. Volcanol. Geotherm. Res., 251, 5–15

Azzaro, R., D'Amico, S., & Tuvè, T., 2011, Estimating the magnitude of historical earthquakes from macroseismic intensity data: new relationships for the volcanic region of Mount Etna (Italy). Seismological Research Letters, 82(4), 533-544.

Azzaro, R., Barberi, G., D'Amico, S., Pace, B., Peruzza, L., & Tuvè, T., 2017, When probabilistic seismic hazard climbs volcanoes: the Mt. Etna case, Italy-Part 1: Model components for sources parameterization. Nat. Hazards Earth Syst. Sci., 17, 1981–1998.

Baratta M., (1901) – I TERREMOTI D'ITALIA – Ed. Bocca, Torino.

Barreca, G., Scarfì, L., Gross, F., Monaco, C., & De Guidi, G. (2019). Fault pattern and seismotectonic potential at the south-western edge of the Ionian Subduction system (southern Italy): New field and geophysical constraints. Tectonophysics, 761, 31-45.

Bella D., Carveni P., Musumeci C. & Gresta S., 1996, Aspetti geomorfologici conseguenti all'attività sismica locale sul basso versante orientale del vulcano Etna. Il Quaternario, 9 (1), 365-368.

Benina A., Imposa S., Gresta S. and Patanè, G. (1984). Studio macrosismico e strumentale di due terremoti tettonici avvenuti sul versante meridionale dell'Etna. Proc. 3° Conv. Ann. GNGTS, 931-940.

Blumetti, A.M., Di Manna, P., Ferreli, L., Fiorenza, D., & Vittori, E., 2007, Reduction of environmental risk from capable faults: The case of the Eastern Etna region (eastern Sicily, Italy), Quaternary International 173–174 (2007) 45–56.

379　Bonforte, A., Guglielmino, F., Coltelli, M., Ferretti, A., & Puglisi, G., 2011, Structural assessment of Mount Etna
380　volcano from Permanent Scatterers analysis. Geochemistry, Geophysics, Geosystems, 12(2).

381　Bonforte, A., Guglielmino, F., & Puglisi, G. (2019). Large dyke intrusion and small eruption: The December 24,
382　2018 Mt. Etna eruption imaged by Sentinel‐1 data. Terra Nova, 31(4), 405-412.

383　Borgia, A., Ferrari, L., & Pasquarè, G., 1992, Importance of gravitational spreading in the tectonic and volcanic
384　evolution of Mount Etna. Nature, 357(6375), 231.

385　Branca, S., Coltelli, M., Groppelli, G., & Lentini, F. (2011). Geological map of Etna volcano, 1: 50,000 scale. Italian
386　Journal of Geosciences, 130(3), 265-291.

387　Branca, S., & Ferrara, V., 2013, The morphostructural setting of Mount Etna sedimentary basement (Italy):
388　Implications for the geometry and volume of the volcano and its flank instability. Tectonophysics, 586, 46-64.

389　Calvari, S., & Groppelli, G. (1996). Relevance of the Chiancone volcaniclastic deposit in the recent history of Etna
390　Volcano (Italy). Journal of Volcanology and Geothermal Research, 72(3-4), 239-258.

391　Carveni, P., and Bella, D. (1994). Aspetti geomorfologici legati ad attività sismica su vulcani attivi: il basso
392　versante orientale dell'Etna come modello di studio. Boll. Acc. Gioenia Sc. Nat, 27(346), 253-285.

393　Carveni P., Bella D., Benfatto S., Maniscalco R., Salleo Puntillo M., & Sturiale G., 2005, Sollevamenti a grande
394　scala e conseguenti fenomeni gravitativi: l'esempio del versante orientale dell'Etna (Sicilia). Il Quaternario, 18
395　(2), 157-171

396　Carveni, P., Filetti, G., & Bella, D., 1997, Aspetti geomorfologici e sismologici connessi a fenomeni di tettonica
397　gravitativa nel basso versante orientale dell'Etna, Geografia Fisica e Dinamica Quaternaria, 20 (1997), 43-49, IT
398　ISSN 0391-9838, 1997.

399　Chiocci, L. F., M. Coltelli, A. Bosman, and D. Cavallaro (2011), Continental margin large-scale instability
400　controlling the flank sliding of Etna volcano, Earth Planet. Sci. Lett., 305, 57–64.

401　Riccardo Civico, Stefano Pucci, Rosa Nappi, Raffaele Azzaro, Fabio Villani, Daniela Pantosti, Francesca R. Cinti,
402　Luca Pizzimenti, Stefano Branca, Carlo Alberto Brunori, Marco Caciagli, Massimo Cantarero, Luigi Cucci, Salvatore
403　D'Amico, Emanuela De Beni, Paolo Marco De Martini, Maria Teresa Mariucci, Paola Montone, Rosella Nave,
404　Tullio Ricci, Vincenzo Sapia, Alessandra Smedile, Gabriele Tarabusi, Roberto Vallone & Alessandra Venuti (2019)
405　Surface ruptures following the 26 December 2018, Mw 4.9, Mt. Etna earthquake, Sicily (Italy), Journal of Maps,
406　15:2, 831-837, DOI: 10.1080/17445647.2019.1683476

407　De Beni, E., Branca, S., Coltelli, M., Groppelli, G., & Wijbrans, J. R. (2011). 40Ar/39Ar isotopic dating of Etna
408　volcanic succession. Italian Journal of Geosciences, 130(3), 292-305.

409　De Novellis, V., Atzori, S., De Luca, C., Manzo, M., Valerio, E., Bonano, M., et al. (2019), DInSAR analysis and
410　analytical modeling of Mount Etna displacements: The December 2018 volcano-tectonic crisis. Geophysical
411　Research Letters, 46, 5817–5827. https:// doi.org/10.1029/2019GL082467

412　Doglioni C., Innocenti F. & Mariotti G., 2001, Why Mt Etna?, Terra Nova, 13, 25-31.

413　Faulkner, D. R., Mitchell, T. M., Healy, D., & Heap, M. J. (2006). Slip on weak faults by the rotation of regional
414　stress in the fracture damage zone. Nature, 444(7121), 922.

415 Ferreli, L., Azzaro, R., Bella, D., Filetti, G., Michetti, A.M., Santagati, F., Serva, L., Vittori, E., 2000. Analisi
416 paleosismologiche ed evoluzione olocenica della fagliazione superficiale lungo la Timpa di Moscarello, Mt. Etna
417 (Sicilia). Bollettino della Societa Geologica Italiana 119 (2000), 251–265.

418 Ferreli, L., Michetti, A.M., Serva, L., Vittori, E., 2002. Stratigraphic evidence of coseismic faulting and aseismic
419 fault creep from exploratory trenches at Mt. Etna volcano (Sicily, Italy). In: Ettensohn, F.R., Rast, N., Brett, C.E.
420 (Eds.), Ancient Seismites. Geological Society of America, Boulder, CO, Special Paper 359, pp. 49–62.

421 Firetto Carlino, M., Cavallaro, D., Coltelli, M., Cocchi, L., Zgur, F., & Patanè, D. (2019). Time and space scattered
422 volcanism of Mt. Etna driven by strike-slip tectonics. Scientific reports, 9(1), 1-15.

423 Ghersi A., Sabatini V., Platania G., 1914, Relazione della commissione per la determinazione delle aree sismiche
424 sulle quali debbono vietarsi le nuove costruzioni nella regione colpita dal terremoto del 7 Maggio in provincia di
425 Catania, Consiglio Superiore dei Lavori Pubblici, Comitato Speciale Roma.

426 Groppelli, G., & Norini, G., 2011, Geology and tectonics of the southwestern boundary of the unstable sector of
427 Mt. Etna (Italy). Journal of Volcanology and Geothermal Research, 208(1-2), 66-75.

428 Groppelli, G., & Tibaldi, A. (1999). Control of rock rheology on deformation style and slip-rate along the active
429 Pernicana Fault, Mt. Etna, Italy. Tectonophysics, 305(4), 521-537.

430 Gross, F., Krastel, S., Geersen, J., Behrmann, J. H., Ridente, D., Chiocci, F. L., Bialas G., Papenberg C., Cukur D.,
431 Urlaub M. & Micallef, A. (2016). The limits of seaward spreading and slope instability at the continental margin
432 offshore Mt Etna, imaged by high-resolution 2D seismic data. Tectonophysics, 667, 63-76.

433 Kettermann, M., & Urai, J. L. (2015). Changes in structural style of normal faults due to failure mode transition:
434 first results from excavated scale models. Journal of Structural Geology, 74, 105-116.

435 Kettermann, M., Weismüller, C., von Hagke, C., Reicherter, K., & Urai, J. L. (2019). Large near-surface block
436 rotations at normal faults of the Iceland rift: Evolution of tectonic caves and dilatancy. Geology, 47, 781–785,
437 https://doi.org/10.1130/G46158.1

438 Laiolo, M., Ripepe, M., Cigolini, C., Coppola, D., Della Schiava, M., Genco, R., ... & Silengo, M. C. (2019). Space-
439 and Ground-Based Geophysical Data Tracking of Magma Migration in Shallow Feeding System of Mount Etna
440 Volcano. Remote Sensing, 11(10), 1182.

441 Lanzafame, G., and Bousquet, J. C. (1997). The Maltese escarpment and its extension from Mt. Etna to Aeolian
442 Islands (Sicily): importance and evolution of a lithosphere discontinuity. Acta Vulcanologica, 9, 113-120.

443 Lentini F., Carbone S. & Guarnieri P., 2006, Collisional and postcollisional tectonics of the Apenninic-Maghrebian
444 orogen (southern Italy). In: Dilek Y. & Pavlides S. (Eds.), Postcollisional tectonics and magmatism in the
445 Mediterranean region and Asia. GSA Special Paper, 409, 57-81.

446 Lo Giudice, E., & Rasa`, R., 1992, Very shallow earthquakes and brittle deformation in active volcanic areas: the
447 Etnean region as example. Tectonophysics 202, 257–268.

448 Lundgren, P., F. Casu, M. Manzo, A. Pepe, P. Berardino, E. Sansosti, & R. Lanari, 2004, Gravity and magma
449 induced spreading of Mount Etna volcano revealed by satellite radar interferometry. Geophys. Res. Lett., 31(4),
450 doi: 10.1029/2003GL018736.

451 Mohammadioun, B. & Serva L. 2001, Stress drop, slip type, earthquake magnitude, and seismic hazard, Bull.
452 Seismol. Soc. Am. 91, no. 4, 694–707.

453 Monaco, C., Catalano, S., Cocina, O., De Guidi, G., Ferlito, C., Gresta, S., Musumeci, C., & Tortorici, L., 2005,
454 Tectonic control on the eruptive dynamics at Mt. Etna Volcano (Sicily) during the 2001 and 2002–2003 eruptions,
455 Journal of Volcanology and Geothermal Research 144 (2005) 211 – 233

456 Monaco, C., De Guidi, G., & Ferlito, C. (2010). The morphotectonic map of Mt. Etna. Italian journal of
457 geosciences, 129(3), 408-428.

458 Monaco, C., Tapponnier, P., Tortorici, L., & Gillot, P.Y., 1997, Late Quaternary slip rates on the Acireale-
459 Piedimonte normal faults and tectonic origin of Mt Etna (Sicily). Earth and Planetary Sciences Letters 147, 125–
460 139.

461 Nappi, R., G. Alessio, G. Gaudiosi, R. Nave, R. E. Marotta,V. Siniscalchi, R. Civico, L. Pizzimenti, R. Peluso, P.
462 Belviso, et al. (2018). The 21 August 2017 MD 4.0 Casamicciola earthquake: First evidence of coseismic normal
463 surface faulting at the Ischia volcanic island, Seismol. Res. Lett. 89, no. 4, 1323–1334, doi: 10.1785/0220180063.

464 Neri, M., Guglielmino, F., & Rust, D., 2007, Flank instability on Mount Etna: Radon, radar interferometry, and
465 geodetic data from the southwestern boundary of the unstable sector. Journal of Geophysical Research:
466 Solid Earth, 112(B4).

467 Nicolich, R., Laigle, M., Hirn, A., Cernobori, L., & Gallart, J. (2000). Crustal structure of the Ionian margin of Sicily:
468 Etna volcano in the frame of regional evolution. Tectonophysics, 329(1-4), 121-139.

469 Norini, G., & Acocella, V. (2011). Analogue modeling of flank instability at Mount Etna: understanding the driving
470 factors. Journal of Geophysical Research: Solid Earth, 116(B7).

471 Patanè, G., & Imposa, S. (1995). Atlante delle isosiste dei terremoti etnei dal 1971 al 1991. CNR-GNGTS, Ist.
472 Geologia e Geofisica Università di Catania, 90 p.

473 Patane' Musumeci A., (1886) – NOTE SUGLI EVENTI SISMICI E VULCANICI DEL 1886 – MANOSCRITTI DI
474 VULCANOLOGIA AUTOGRAFI

475 Platania G., (1915) - SUL PERIODO SISMICO DEL MAGGIO 1914 NELLA REGIONE ORIENTALE DELL' ETNA - Tip.
476 Orario delle Ferrovie.

477 Riuscetti, M., Distefano, R., 1971. Il terremoto di Macchia (Catania). Bollettino di Geofisica Teorica ed Applicata,
478 13 (51), 150-164.

479 Rovida, A., Locati, M., Camassi, R., Lolli, B., & Gasperini, P. (2016). CPTI15, the 2015 version of the Parametric
480 Catalogue of Italian Earthquakes, Istituto Nazionale di Geofisica e Vulcanologia (INGV), Rome. doi:
481 10.6092/INGV. IT-CPTI15.

482 Ruch, J., Pepe, S., Casu, F., Acocella, V., Neri, M., Solaro, G., & Sansosti, E. (2012). How do volcanic rift zones
483 relate to flank instability? Evidence from collapsing rifts at Etna. Geophysical Research Letters, 39(20).

484 Sabatini V., (1915) - NOTE SUL TERREMOTO DI LINERA DELL'8 MAGGIO 1914. - Bollettino del R. Comitato
485 Geologico D'Italia - vol. 45 (4° della Va serie)

486   Silvestri O., (1879a) – FENOMENI DELL'ETNA SUCCESSIVI ALL'ULTIMA ERUZIONE – in Boll. Del Vul. It., a 6, pp. 118
487   – 124, Roma.

488   Silvestri O., (1879b) – SULLA DOPPIA ERUZIONE DELL'ETNA SCOPPIATA IL 26 MAGGIO 1879, RAPPORTO ALLE LL.
489   EE. I MINISTRI DELL'INTERNO, DELL'ISTRUZIONE PUBBLICA E DI AGRICOLTURA, INDUSTRIA E COMMERCIO -
490   Catania.

491   Solaro, G., Acocella, V., Pepe, S., Ruch, J., Neri, M., & Sansosti, E. (2010). Anatomy of an unstable volcano from
492   InSAR: Multiple processes affecting flank instability at Mt. Etna, 1994–2008. Journal of Geophysical Research:
493   Solid Earth, 115(B10).

494   Tarquini, S., Vinci, S., Favalli, M., Doumaz, F., Fornaciai, A., & Nannipieri, L. (2012). Release of a 10-m- resolution
495   DEM for the Italian territory: Comparison with global-coverage DEMs and anaglyph-mode exploration via the
496   web. Computers & Geosciences, 38(1), 168–170. https://doi.org/10.1016/j.cageo.2011.04.018

497   Tibaldi, A., & Groppelli, G., 2002, Volcano-tectonic activity along structures of the unstable NE flank of Mt. Etna
498   (Italy) and their possible origin. J. Volcanol. Geotherm. Res. 115, 277– 302.

499   Urlaub, M., Petersen, F., Gross, F., Bonforte, A., Puglisi, G., Guglielmino, F., ... & Kopp, H. (2018). Gravitational
500   collapse of Mount Etna's southeastern flank. Science advances, 4(10), eaat9700.